Kinetics of large B clusters in crystalline and preamorphized silicon

Maria Aboy,[1,a)] Lourdes Pelaz,[1] Elena Bruno,[2] Salvo Mirabella,[2] and Simona Boninelli[3,b)]
[1]*Universidad de Valladolid, Campus Miguel Delibes, 47011 Valladolid, Spain*
[2]*MATIS-IMM-CNR, Via Santa Sofia 64, I-95123 Catania, Italy*
[3]*Italian Institute Technol. Via Morego 30, I-16163 Genova, Italy*

(Received 28 July 2011; accepted 11 August 2011; published online 14 October 2011)

We present an extended model for B clustering in crystalline or in preamorphized Si and with validity under conditions below and above the equilibrium solid solubility limit of B in Si. This model includes boron-interstitial clusters (BICs) with B_nI_m configurations—complexes with n B atoms and m Si interstitials—larger ($n > 4$), and eventually more stable, than those included in previous models. In crystalline Si, the formation and dissolution pathways into large BICs configurations require high B concentration and depend on the flux of Si interstitials. In the presence of high Si interstitial flux, large BICs with a relatively large number of interstitials ($m \geq n$) are formed, dissolving under relatively low thermal budgets. On the contrary, for low Si interstitial flux large BICs with few interstitials ($m \ll n$) can form, which are more stable than small BICs, and whose complete dissolution requires very intense thermal budgets. We have also investigated the kinetics of large BICs in preamorphized Si, both experimentally and theoretically. B was implanted at a high-dose into preamorphized Si, and the B precipitation was studied by transmission electron microscopy and by sheet resistance and Hall measurement techniques. A simplified model for B clustering and redistribution in amorphous Si is proposed, including the experimental value for the B diffusivity in amorphous Si and the energetics of BICs. Our model suggests that B_2, B_3I, B_4I and B_4I_2 clusters are the most energetically favored configurations, with relative abundance depending on B concentration. After recrystallization, thermal anneals up to 1100 °C evidence that BICs evolve under very low flux of Si interstitials under the particular experimental conditions considered. Simulations indicate that for very high B concentrations and low Si interstitial flux a significant fraction of the initial small BICs evolves into larger and very stable BIC configurations that survive even after intense thermal budgets, as confirmed by energy filtered transmission electron microscopy analyses. The correlation between simulations and Hall measurements on these samples suggest that hole mobility is significantly degraded by the presence of a high concentration of BICs. © *2011 American Institute of Physics*. [doi:10.1063/1.3639280]

I. INTRODUCTION

The progressive miniaturization of Si-based complementary metal-oxide-semiconductor (CMOS) devices increasingly demands a large number of technological challenges that make the fabrication of integrated circuits very complex. At the junction level, the International Technology Roadmap for Semiconductors (ITRS) indicates as one of the most challenging requirements the fabrication of ultra-shallow source/drain (S/D) extension regions and extremely high electrically active doping levels in order to control short-channel effects (SCE) and maximize drive current for higher switching speed.[1]

Junctions are generally formed by ion implantation as this is a conventional and well established technique to introduce dopants in semiconductors in a controlled way. Particularly challenging is the fabrication of highly electrically active p + /n junctions. For that purpose B is implanted in Si at very high doses, resulting in B concentrations that significantly exceed its equilibrium solid solubility limit (s.l.) in Si.[2] As a consequence of such a high B concentration as well as the lattice damage resulting from ion implantation, electrically inactive boron-interstitial clusters (BICs) are formed, making the fabrication of low-resistivity junctions difficult.[3–5] In fact, when B is implanted in crystalline Si the formation of BICs is difficult to avoid because they form rapidly,[4,5] leading to active B concentration levels well below equilibrium solid solubility (s.l.). BICs dissolution (and thus, B reactivation) generally requires the use of high thermal budgets, but this process is accompanied by significant B diffusion.[6] The difficult trade-off between maximum dopant activation and shallow and abrupt junction formation becomes more and more challenging as device dimensions shrink. The increasingly demand for highly doped and ultra-shallow junctions has extended the use of low-temperature solid phase epitaxial regrowth (SPER) of preamorphized Si since it has been proved to result in metastable high activation levels of B (up to concentrations typically around $1.5\text{-}3.0 \times 10^{20}$ B/cm^3, well above the equilibrium s.l. at the low temperatures typically used in this technique) with minimal dopant diffusion.[7,8] This approach also benefits from the complete suppression of channeling of B beams, since it is implanted in amorphous Si.

a)Author to whom correspondence should be addressed. Electronic mail: marabo@tel.uva.es.
b)Present address: MATIS-IMM-CNR, Via Santa Sofia 64, I-95123 Catania, Italy.

 © 2011 American Institute of Physics

Author complimentary copy. Redistribution subject to AIP license or copyright, see http://jap.aip.org/jap/copyright.jsp

For B concentrations higher than this metastable value complete electrical activation is not possible and, as a result, BICs are formed in the preamorphized region after SPER.[7,8] Moreover, after SPER residual end-of-range (EOR) defects beyond the amorphous-crystalline interface may remain if the thermal budget is too low, which is known to degrade dopant activation (through the growth of BICs resulting from SPER) and junction depth during subsequent thermal annealing.[5,7,8] Therefore, a deep understanding of mechanisms associated to the formation and dissolution of BICs is essential to control and optimize B electrical activation in both crystalline and preamorphized Si in order to improve device performances. Some not negligible gaps still remain opened between the experimental evidences of BICs and their modeling, such as the BIC size, their formation in the amorphous Si and transition into crystalline Si, or their effects on the electrical properties. Thus, a significant revision of the previous modeling for B clustering in Si is required.

Mechanisms for B clustering in crystalline Si have been extensively analyzed in the literature and several models have been proposed, based on theoretical calculations[9–12] or inverse modeling over experimental data.[4,5] Those models for BICs were based on the formation of complexes of B atoms and interstitials (Is) that generally contain only few B atoms (typically from one up to four B atoms associated to Is) since no direct experimental evidences of large size clusters were available. However, quite large BICs have been recently detected by transmission electron microscopy (TEM) analyses under conditions of very high B concentrations.[13,14] Based on weak-beam-dark-field (WBDF) investigations, Cristiano *et al*. have reported experimental data based on high-dose ultra-low energy B implants in crystalline Si that evidenced the formation of large BICs after a low-temperature annealing that disappeared after high temperature spike anneals.[13] Boninelli *et al*. presented studies focusing on the thermal evolution of BICs formed by Si implantation in crystalline Si samples containing a buried, highly doped B profile and they also showed large BIC formation.[14] Moreover, similar experiments reported by De Salvador *et al*. revealed the existence of two main kinetics paths for BICs dissolution, a faster dissolution path and a slower one.[15] They suggested that small BICs undergo the faster dissolution path whereas large and more stable BICs would be subject to the slower dissolution path. As a consequence, current models for BICs need to be extended in order to include the possibility of growth into these larger and eventually more stable configurations of BICs.

The situation when B is implanted in preamorphized Si is significantly different than in crystalline Si. Experimental secondary-ion-mass spectrometry (SIMS) profiles evidence an immobilization of B atoms for concentrations above $\sim 2 \times 10^{20}$ B/cm^3 after low temperature SPER.[7,8] At the same time, lower B concentrations show B diffusion in amorphous Si during recrystallization.[16] Moreover, sheet resistance measurements after low temperature recrystallization are also consistent with maximum levels of B activation of around $\sim 2 \times 10^{20}$ B/cm^3.[7,8] All these observations support the hypothesis of formation of immobile BICs in amorphous Si at B concentrations higher than that limit value, as experimentally verified by De Salvador *et al*.[17] By using theoretical calculations, Mattoni and Colombo have characterized the formation kinetics of some BICs during recrystallization and found that B_2I, B_3I and B_4I_2 configurations could play the major role in the evolution of recrystallized B-doped Si.[18] However, there are still some uncertainties about the configurations of BICs after recrystallization and the kinetics of their nucleation in amorphous Si is generally not modeled in detail.

Although such BICs could have a not negligible effect on the mobility of charge carriers, still it has been disregarded. Generally the assessment of the electrically active dopant dose (N_a) is based on the experimental determination of the sheet resistance (R_S) usually by four-point probe measurements, through the following expression:[8]

$$N_a \approx \left(q\mu_p R_s\right)^{-1} ohm/sq, \tag{1}$$

where q is the elementary charge and μ_p represents the hole mobility. In such a way, it is assumed that μ_p only depends on the electrically active dopant concentration.[19] Therefore, the evolution of N_a is commonly understood in terms of the evolution of R_S, showing an inverse trend, whereas changes in μ_p are considered practically negligible for the variation of dopant concentration that typically occurs in experiments.[8] Alternatively, both the N_a and μ_p values can be experimentally directly determined by using Hall measurements. Hall concentration and Hall mobility values could be converted into carrier concentration and drift mobility, respectively, by using the appropriate Hall scattering factor (r_H).[20] As we will show in this article, this type of measurements suggests that the previously mentioned assumption, which considers negligible changes in μ_p, could be erroneous under very high B concentration conditions.

In this article we use atomistic simulations to gain physical understanding of the mechanisms associated to B clustering that leads to B deactivation in Si in highly B-doped junctions both in crystalline and preamorphized Si. In our model we simulate ion implantation using the binary collision approximation, and the kinetics and interactions of dopants and defects through a non-lattice kinetic Monte Carlo code. As described in previous works,[4,5,21] parameters that define the atomic interactions, such as diffusivities, binding energies, capture radius, etc., are derived from theoretical calculations[9–12,22–24] or dedicated experiments.[4,5,25,26] In this article we focus in the novel aspects of our B clustering model which is proposed in order to account for the experimentally observed growth of small BICs into larger BIC configurations under very high B concentration conditions. In order to evaluate the validity and implications of the proposed model, we have analyzed different experiments reported in the literature in which the formation of large BICs has been postulated for high B concentration profiles in crystalline Si under different damage conditions. Furthermore, we present for the first time experimental evidences of formation of large and observable BICs for high B concentration profiles implanted in preamorphized Si. The analysis of these new experimental data combined with kinetic Monte Carlo simulations suggest that hole mobility could be largely affected by the presence of BICs.

Author complimentary copy. Redistribution subject to AIP license or copyright, see http://jap.aip.org/jap/copyright.jsp

In the following section, the model extension for large BICs in crystalline Si is presented and compared with literature data. In Sec. III, a novel experiment evidencing the formation of BICs in amorphous Si and their transition to the recrystallized Si as well as their posterior evolution during subsequent anneals is reported together with a proper model, paying also attention to the effect of BICs on the hole mobility.

II. BICs KINETICS IN CRYSTALLINE SILICON: AN EXTENDED MODEL FOR LARGE BICs

Previous models for B clustering included complexes of n B atoms and m Is, B_nI_m, that contain only few atoms, generally up to four B atoms and several I defects.[4,5,9–12] However, recent experiments have evidenced the formation of BICs larger than generally assumed (even observable by electron microscopy techniques) if B concentrations higher than $\sim 10^{20}$ B/cm^3 are present.[13–15] Experiments also indicate that these "observable" BICs could be very stable under some particular conditions.[14,15] For this reason, we have developed a new extended model for BICs, which includes larger BICs than those considered in previous models. Such a model will be presented in the next Sec. II A, while it will be applied to literature experimental data dealing with large BICs containing few (Sec. II B) or many (Sec. II C) Is.

A. Physical modeling

Based on experimental evidences we proposed the existence of two main species of BICs: the small BICs included in previous models ($n \leq 4$) and a new type of larger BICs ($n > 4$) that only form in the presence of very high B concentrations and that eventually could be very stable. Schematic diagrams of Fig. 1 include the energetics of the several BIC configurations (Fig. 1(a)) and the main features of the proposed model (Fig. 1(b)). These energies, $E_{tot}(B_nI_m)$, are referred to the perfect lattice, thus configurations with low energy correspond to more stable defects whereas

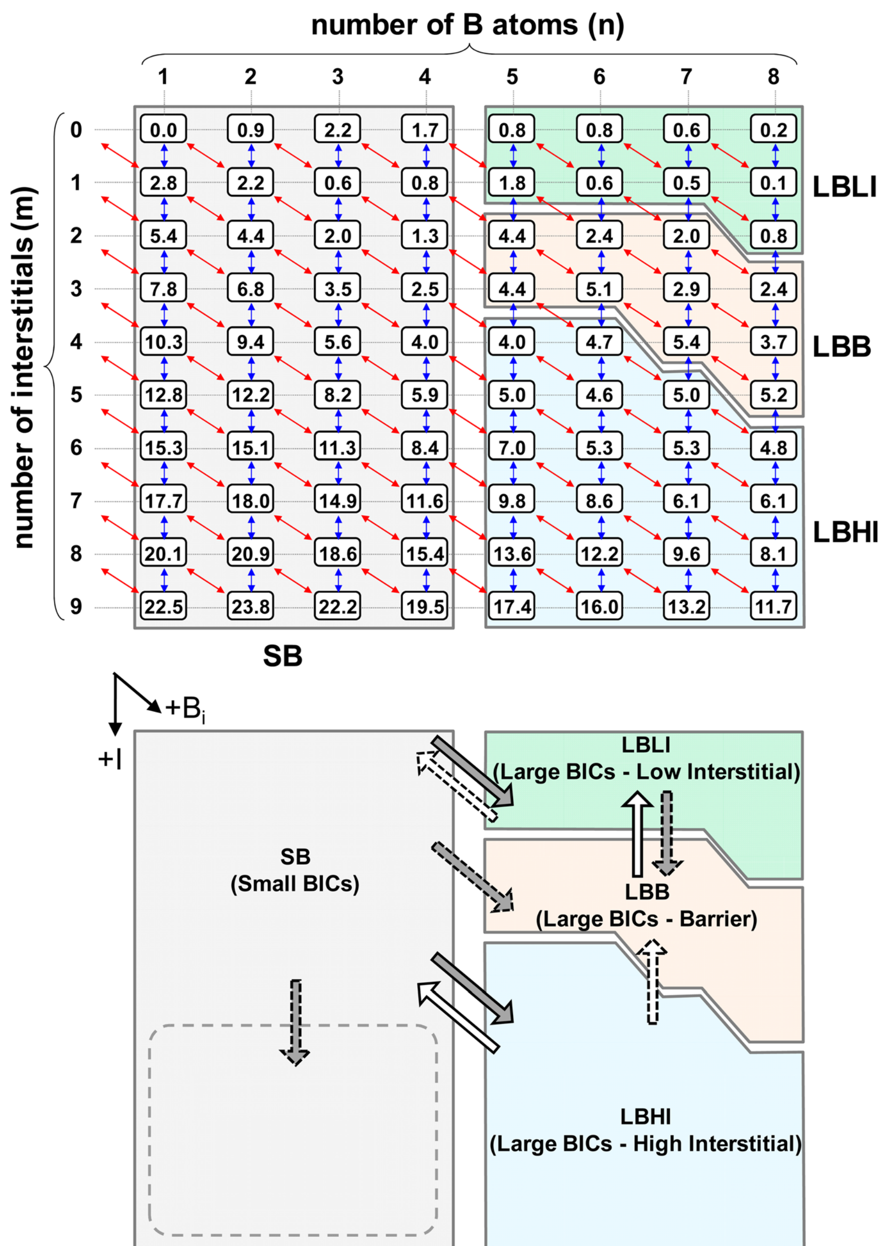

FIG. 1. (Color online) Schematic representations of (a) the energetics of the several BIC configurations (B_nI_m) referred to the perfect lattice and (b) the main features of the proposed model which includes four main regions. (a) Oblique (red) and vertical (blue) arrows represent the formation/dissolution paths for the different configurations through the trapping/emission of mobile species boron-interstitial (B_i) and Si interstitial (I), respectively. (b) Gray and white arrows distinguish between formation and dissolution paths, respectively, whereas solid and dashed arrows indicate high and low probability paths, respectively.

Author complimentary copy. Redistribution subject to AIP license or copyright, see http://jap.aip.org/jap/copyright.jsp

configurations with high energy are associated to less stable defects. These energies have been obtained by fitting models to different sets of experimental data and taking main indications of theoretical calculations as a reference.[9–12] Oblique (red) and vertical (blue) arrows represent in our model the formation/dissolution paths for the different B_nI_m configurations through the trapping/emission of mobile species boron-interstitial (B_i) and Si interstitial (I), respectively, controlled by the following reactions:

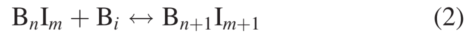

$$B_nI_m + B_i \leftrightarrow B_{n+1}I_{m+1} \quad (2)$$

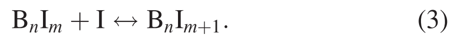

$$B_nI_m + I \leftrightarrow B_nI_{m+1}. \quad (3)$$

Based on these reactions, adding a B_i pair or an I to a preexisting B_nI_m cluster entails a reduction in the energy of the overall system given by the following expressions, respectively:

$$E^{Bi}_{bind}(B_{n+1}I_{m+1}) = E_{tot}(B_nI_m) + E_{tot}(B_i) - E_{tot}(B_{n+1}I_{m+1}) \quad (4)$$

$$E^{I}_{bind}(B_nI_{m+1}) = E_{tot}(B_nI_m) + E_{tot}(I) - E_{tot}(B_nI_{m+1}). \quad (5)$$

where E_{tot}(I) represent the formation energy of the free Si Is whose value is 3.8 eV in our model, according to theoretical calculations.[22,25] Negative values for these energies indicate that a barrier for the trapping of the particular mobile specie from the B_nI_m cluster exists. In contrast, positive values indicate that the trapping of the particular mobile specie is energetically favorable, and the higher is the energy value the more stable the resulting BIC is. For example, the addition of an I to B_7I_5 is highly favored since the energy of B_7I_6 is only 0.3 eV larger than that for B_7I_5, so the energy balance gives + 3.5 eV.

In order to provide a description of the features of the model we have defined four main regions. Region SB (Small BICs) corresponds to configurations included in our previous model for small BICs ($n < 4$) whereas regions Large BICs—Low Interstitial (LBLI), Large BICs—Barrier (LBB) and Large BICs—High Interstitial (LBHI) represent different regions within BIC configurations with larger number of B atoms. In order to limit the number of parameters in the model, we have considered large BICs up to eight B atoms.[27] Experimental observations indicated that large BICs only form in the presence of very high B concentrations (well above equilibrium solid solubility) whereas for low and medium B concentrations the BIC evolution follows a classical pathway.[15] In order to make our model compatible with previous works for low and medium B concentrations we propose the existence of intermediate BIC configurations (B_5I_m) among the small BICs included in previous models and large BICs, being these intermediate configurations less energetically favored. For this purpose, we consider that energies of B_5I_m configurations are relatively higher than those for B_4I_{m-1} configurations. Thus the probability of growing of small BICs through the forward reaction $B_4I_m + B_i \leftrightarrow B_5I_{m+1}$ is very low, preventing the formation of large BICs for low and medium B concentrations. Only in the presence of very high B concentrations, BICs could evolve toward large BICs. Figure 1(b) schematizes the main characteristics of the four different regions considered in our model. Gray and white arrows distinguish between growth and dissolution paths, respectively, whereas solid and dashed arrows indicate high and low probability paths, respectively. Main features associated to these regions are described below.

- Region SB corresponds to our previous model for BICs, which includes configurations up to four B atoms whose validity was demonstrated in several previous works for low and medium B concentration profiles under diverse experimental conditions.[5] Other authors reported slightly different values for the energetic of small BICs although they agree on the overall description of the system.[9–12] The mechanisms for BIC formation and dissolution within the small BICs region in our model have been described in a previous work.[5] Note that small BICs with large amount of Is (dashed region in Fig. 1(b)) have very high energy in the model and thus, are quite unstable and have very low probability to form. Concerning the evolution from small to large BIC regions, note that the growth into configurations within the LBB region described by Eq. (2) is not energetically favored according to Eq. (4) (since negative values are obtained). The evolution from small BICs toward regions LBHI and LBLI (described in the following), and thus, the growth into these regions is possible according to Eq. (4), although only in the presence of high B concentrations (since in general the E^{Bi}_{bind} values are not very high).
- Region LBHI includes large BICs with large amount of Is. These BICs could form rapidly under high B concentration conditions in the presence of a high flux of Si Is (as it occurs for instance during high-dose low-energy B implantation). Within region LBHI, configurations with $m > n$ have relatively high total energy (thus, these configurations are quite unstable). Moreover, the evolution within region LBHI toward configurations with $m \leq n$ by the emission of Is entails an energy increase (given by Eq. (5)) generally higher than the emission of B_i (given by Eq. (4)), which makes the emission of B_i more likely than the emission of Is. Note also that the evolution from region LBHI toward region LBB by the emission of Is entails a significant energy increase which makes this evolution very improbable. All these features favor the formation of large BIC configurations with $n \approx m$. Since these large BIC configurations have relatively high energies in the model, once they form they could easily evolve toward small BICs through B_i emission at relatively low thermal budgets. This is compatible with experimental observations reported by Cristiano *et al*. in which a high-dose low-energy B implant in crystalline Si created a high B concentration profile overlapping with a highly damaged region that contain a high concentration of Si interstitials.[13] These experiments evidenced a rapid formation of large BICs, visible by WBDF imaging after 650 °C, 10 s annealing, which become undetectable by WBDF after high temperature spike anneals.
- Region LBLI includes large BICs with low amount of Is ($m \ll n$). These configurations could form under high B concentration conditions in the presence of a low flux of Si Is, whether by the interaction of low Si interstitial content B_4I_m configurations with B_i pairs (through forward reaction Eq. (2)) or by the emission of Is from configurations of region LBB (through reverse reaction Eq. (3)). These

Author complimentary copy. Redistribution subject to AIP license or copyright, see http://jap.aip.org/jap/copyright.jsp

configurations are characterized for very low total energies. Therefore, these BICs are quite stable and their dissolution requires intense thermal budgets. This is compatible with experiments reported by De Salvador *et al.* that suggested the formation of very stable large BICs for high B concentration B marker layers that do not overlap with a high damage region resulting from a Si implant (thus, B atoms are in the presence of a low flux of Si Is).[15] They showed that large BICs formed under these conditions could be more stable than usual small BICs, and they could even survive after very intense anneals, which causes a slowing down in the BIC dissolution rate when larger BICs are present.

- Region LBB includes large BICs with intermediate amount of Is. This region represents a set of configurations among regions LBHI and LBLI that have relatively low probability to form, as discussed before. Thus, this region could be considered as a sort of barrier that makes the evolution from less stable configurations of the region LBHI toward more stable configurations of the region LBLI (through the emission of Is) difficult. Thus, BICs in region LBHI tend to return to small BICs of region SB rather than evolving toward configurations within region LBB. This is compatible with experimental observations reported by Cristiano *et al.* which evidence that large BICs dissolve after a high temperature spike annealing without the need of intense anneals as it would be required if BICs had evolved toward configurations within region LBLI.[13] Note that the evolution into configurations within the region LBB only has significant probability in term of energetics from configurations within the region LBLI by forward reactions Eq. (2) and Eq. (3). However, these configurations tend to emit Is quickly in order to evolve toward more stable configurations of the region LBLI.

B. Large BICs with low I content

In order to evaluate the new model including large BICs, we firstly investigate the formation and dissolution mechanisms of BICs induced by Si ion implantation into samples with substitutional B profiles at concentrations either below or above s.l. (at 815 °C s.l. $\sim 3.8 \times 10^{19}$ B/cm^3 [2]). For this purpose we considered the experiments reported by De Salvador *et al.* [15]. Fully substitutional box-shaped B profiles at a depth of 220 nm and at concentrations of 1×10^{19} B/cm^3 (labeled as sample S1), 5×10^{19} B/cm^3 (labeled as sample S2) and 2×10^{20} B/cm^3 (labeled as sample S3), were implanted with 20 keV Si ions (projected range around 30 nm) at the nonamorphizing dose of 1×10^{14} ions/cm^2. Then, a first rapid thermal annealing step at 815 °C for 5 min was performed (using a 50 °C/s ramp-up rate) in order to investigate the formation and eventual growth of BICs. Later, all samples were given an additional second annealing step at 900 °C in order to analyze the subsequent evolution and eventual dissolution of BICs formed during the first annealing step. These experimental conditions allow us to investigate the evolution of BICs for different B concentration profiles in the presence of a low flux of Si Is, since the highly damaged region created by the Si implant does not overlap with the initially substitutional B profile.

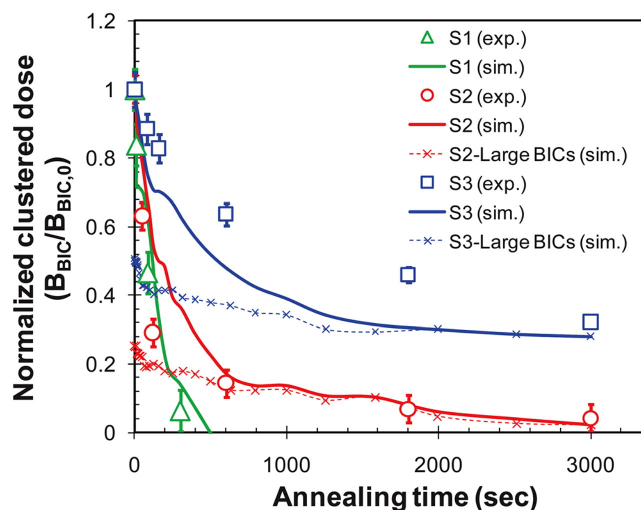

FIG. 2. (Color online) Experimental data [15] and simulation results for the evolution of the normalized clustered B dose as a function of the second annealing step time at 900 °C for samples S1 (1×10^{19} B/cm^3 B box), S2 (5×10^{19} B/cm^3 B box) and S3 (2×10^{20} B/cm^3 B box) implanted with 20 keV, 10^{14} Si ions/cm^2. The inclusion of very stable BICs with more than four B atoms in the model—represented as normalized dose of large BICs in the figure—allow us to capture the firstly faster and later slower regimes of dissolution observed experimentally for high B concentration samples S2 and S3.

Figure 2 plots the experimental values (symbols) for the total clustered B dose (B_{BIC}) as a function of annealing time at 900 °C for all samples.[15] These values were normalized to the clustered B dose resulting from the first annealing step at 815 °C ($B_{BIC,0}$). Experimental data were extracted by De Salvador *et al.* from the SIMS profiles[15] by using the fitting procedure described in Ref. 28. Along with these extracted values we include in Fig. 2 the simulated values for the total clustered dose (solid lines) as well as the simulated dose of B atoms stored in large BICs (dashed lines) resulting from the second annealing step at 900 °C (note that large BICs are not obtained in simulations for sample S1). All values extracted from simulations were also normalized to the simulated clustered B dose obtained just after the first annealing step process for each respective sample. As discussed in Ref. 15 experimental data reveals that whereas the BIC dissolution in sample S1 (triangles) is well described by a single exponential decay, samples S2 (circles) and S3 (squares) clearly present two stages in the dissolution. The first stage is quite fast, whereas the second stage is much slower and involves a smaller fraction of the initial clustered dose $B_{BIC,0}$. Moreover, in the case of sample S3, the fraction of the clustered B dissolving through the slower process is much higher, and the dissolution rate is very similar to the slowly dissolving BICs of the sample S2.

Simulations performed by using our previous model for BICs (not shown in the figure), which only include BICs up to four B atoms, are unable to reproduce the complete set of experimental data. Thus, simulations using the previous model lead to results similar to experiments for sample S1. However, for samples S2 and S3 simulations performed by using our previous model for BICs lead to initial clustered doses smaller than those obtained by experiments. Moreover, resulting BICs dissolve with only a fast decay rate in

Author complimentary copy. Redistribution subject to AIP license or copyright, see http://jap.aip.org/jap/copyright.jsp

simulations performed with our previous model, i.e., they do not predict the slow dissolution rate and, as a result, BICs completely dissolve faster than expected. In contrast, our extended model for B clustering, which includes large BICs, allows us to reproduce experimental data for all samples as it can be seen in Fig. 2. Simulations indicate that the first annealing step at 815 °C fully dissolves the Si interstitial and vacancy defects and injects Si Is toward the B box which interact with B atoms causing the formation of BICs in all samples. Simulations show that only a small fraction of the total B dose evolve to BICs, due to these particular conditions in which the B profile do not overlap the high damage region resulting from the Si implant. Thus, the Si interstitial supersaturation set by the implant damage lead to clustered doses of 6.5×10^{13} (S3), 2.2×10^{13} (S2) and 4.6×10^{12} B_{BIC}/cm^2 (S1) after the first annealing step at 815 °C (in agreement with reported experimental values[15]), which implies around 17%, 27%, and 33% of the total B dose, respectively. Our simulations also show that no large BICs are formed in sample S1, due to the low B concentration. Thus, the decrease of the clustered dose during the second annealing step at 900 °C for S1 is only controlled by the dissolution of small BICs, mainly by the emission of B_i from B_3I clusters (with an activation energy ~3.8 eV, in agreement with experimental observations[15]). In fact, it is worthy to note that simulation results obtained by the full extended B clustering model for sample S1 were almost identical to those obtained with our previous model for BICs, without including large BICs (not shown in the figure). In contrast, for samples S2 and S3 simulations show that Si Is injected from the damaged region (during the first annealing step at 815 °C) lead to the growth of small BICs, and that a fraction of them evolves into large and more stable BICs (around 25 and 50% of $B_{BIC,0}$ for samples S2 and S3, respectively).

In order to gain a deeper insight into situations in which large BICs are involved we represent in Fig. 3 the evolution of the doses of electrically active B, Si Is stored in Si interstitial defects, B atoms and Is stored in BICs (both small and large BICs) and B atoms and Is stored in large BICs, all of them extracted from the simulation for sample S3. Figure 3(a) includes the evolution during the Si implant, whereas Figs. 3(b) and 3(c) plot the evolution during first and second step anneals at 815 °C and 900 °C, respectively. Figure 3(a) shows that, during the Si implantation process, excess Si Is evolve to Si interstitial defects (small Si interstitial clusters) and that, at the same time, a small fraction of the initially active B atoms (~15%) grow into small BICs. Since the highly damaged region resulting from the Si implant (Si Is and vacancies) does not overlap with the B profile, the formation of BICs occurs through the injection of Si Is coming from the damage region to the B profile. According to previous work, under these conditions the flux of Si Is is not enough to form BICs with a high interstitial content.[5] In fact, Fig. 3(a) shows that the dose of Is trapped in BICs is significantly smaller than the dose of B atoms in BICs, indicating that BICs are formed through the low interstitial content pathway.[5] As a result, after the Si implant around 85% of BICs are in the form of B_2I_m, most of them as B_2I (which form by reaction $B + B_i \rightarrow B_2I$).

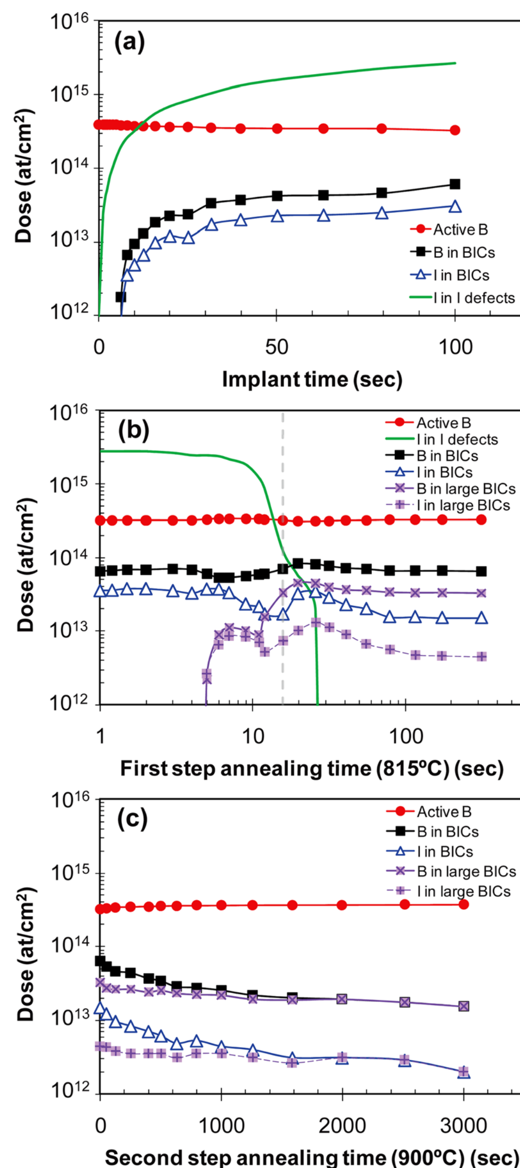

FIG. 3. (Color online) Simulated time evolution of the doses of electrically active B, Si Is stored in Si interstitial defects, B atoms and Is stored in BICs (both small and large BICs) and B atoms and Is stored in large BICs, as extracted from simulation for sample S3. This figure includes the evolution of doses during (a) the 20 keV, 10^{14} Si ions/cm^2 implant at room temperature, (b) the first step annealing at 815 °C for 5 min, and (c) the second step annealing at 900 °C. Dashed line represents the instant at which the end of the ramp up (at 50 °C/s) to the target temperature of the first step annealing at 815 °C is reached.

During the first annealing step at 815 °C (Fig. 3(b)) BICs tend to grow toward configurations with larger amount of B atoms at the same time that Si interstitial defects dissolve. Thus, after the ramp up of the first annealing step (dashed line in Fig. 3(b)), the percentages of B_3I_m, B_4I_m and $B_{n>4}I_m$ configurations are around 9%, 60%, and 31%, respectively. Again these configurations have a low Si interstitial content ($m < 3$). In particular small BICs are mainly in the form of B_3I, B_4I and B_4I_2 whereas large BICs are in the form of B_n and B_nI configurations, i.e., very stable large BICs of the region LBLI in Fig. 1. This is also in agreement with experimental findings. TEM analyses performed on those samples, linked to experimental extraction of the Si Is flux,

Author complimentary copy. Redistribution subject to AIP license or copyright, see http://jap.aip.org/jap/copyright.jsp

revealed that the average composition of these BICs results to be shifted toward B rich precipitates.[14]

A detailed study of the evolution of BICs during the ramp up and the early stages of the 815 °C annealing has allowed us the identification of the mechanisms of growth into large BICs according to our model. Simulations indicate that 5 s after the beginning of the anneal ramp up (when the annealing temperature is about 280 °C) approximately a 16% of the BICs evolved toward B_4I_m configurations (mainly B_4I_2 although some of them have more Is such us B_4I_3 or B_4I_4). Few seconds later a small fraction of B_4I_m configurations grow into larger BICs through the interaction with B_i. Figure 3(b) shows that initially the dose of Is stored in large BICs is practically equal to the dose B atoms stored in these BICs. Thus, initially large BICs mainly consist of configurations with $n \approx m$ such us B_5I_4, B_5I_5, B_6I_4, B_6I_5… (within the region LBHI in Fig. 1). This partial evolution toward large configurations is possible due to the presence of high B concentrations and the flux of Si Is coming from Si interstitial defects. However, as the annealing temperature slightly increases during the ramp up to the target temperature, these large configurations quickly return to small BICs, as discussed in Sec. II A. On the other hand, simulations show that the eventual injection of vacancies from the damage region favors the evolution of some B_4I_m toward configurations without Is which easily evolve toward more stable configurations within the region LBLI of BICs (through forward reaction Eq. (2)). Thus, at the end of the ramp up of the first annealing step a considerable dose of B atoms are stored in large BICs that contain a dose of Is significantly smaller. Moreover, Si interstitial defects have practically dissolved, which leads to a significant reduction in the flux of Si Is. As a result, these more stable BICs formed during the ramp up easily grow during the annealing at 815 °C toward larger and very stable BICs within region LBLI through reactions $B_nI + B_i \rightarrow B_{n+1}I_2 \rightarrow B_{n+1}I$ (since B_nI_2 configurations emit Is rapidly, as discussed in Sec. II A). Thus, after the first annealing step at 815 °C around a 50% of clustered B atoms are stored in large BICs as it can be observed in Fig. 3(b). On the other hand, small BICs tend to evolve during the annealing at 815 °C toward B_3I which is a quite stable configuration in the model. As a result, after the first annealing step at 815 °C around 30% of total BIC configurations are large BICs (mainly in the form of B_n and B_nI configurations) whereas a 70% of BICs are in the form of B_3I. Finally, during the second annealing step at 900 °C (Fig. 3(c)), the initial fast decay of B atoms stored in BICs corresponds to the dissolution of small BICs, whereas the dose of large BICs remains almost constant. Once small BICs fully dissolve the BIC dissolution rate is controlled by the evolution of very stable large BICs of the region LBLI. As a result, once small BICs completely dissolve the dissolution rate of BICs significantly slows down.

C. Large BICs with high I content

Formation of BICs larger than conventionally considered has been also reported by Cristiano *et al*. under quite different conditions.[13] In those experiments, crystalline Si samples were implanted with 500 eV B ions to a dose of 1×10^{15} B/cm^2 (typical conditions required for the formation of ultra-shallow and extremely highly doped p+/n junctions). Subsequent to a 650 °C 10 s pre-stabilization annealing step (using a 50 °C/s ramp-up rate), samples were then spike annealed at 1050 °C and 1100 °C using a 250 °C/s ramp-up rate. Under these experimental conditions the situation is quite different from the one previously analyzed since the highly damaged region (Si Is and vacancies) resulting from the B implant overlaps with the implanted high B concentration profile. Figure 4 shows the B profiles obtained after the implantation process and after the 1050 °C and 1100 °C spike anneals (including the pre-stabilization annealing step at 650 °C) extracted from simulations performed with the extended model for BICs. Simulations evidence the presence of a characteristic B concentration peak at a depth of ∼2 nm, in agreement to experiments, typically associated to the formation of BICs. For more intense thermal budget, the B concentration peak decreases and the tail region of the B profile broadens, similarly to experimental SIMS profiles.[13] Thus, experimental junction depths at 10^{19} B/cm^3 were ∼30 and 44 nm for 1050 °C and 1100 °C spike anneals,[13] respectively, whereas simulations lead to junction depths of 28.5 and 47.2 nm, respectively, in good agreement to experimental data. Moreover, experimental values for B peak concentration were approximately 1×10^{21} and 5.2×10^{20} B/cm^3 for 1050 °C and 1100 °C spike anneals,[13] respectively, whereas simulations lead to B peak concentrations of 9.9×10^{20} and 6.7×10^{20} B/cm^3.

In order to obtain a better understanding of this situation we include in Fig. 5 the simulated evolution of the doses of electrically active B, Si Is stored in Si interstitial defects, B atoms and Is stored in BICs (both small and large BICs) and B atoms and Is stored in large BICs, all of them extracted from the simulation of the sample spike annealed at 1050 °C. Figure 5(a) includes the evolution during the B implant, whereas Figs. 5(b) and 5(c) plot the evolution during first and second step anneals at 650 °C and 1050 °C, respectively.

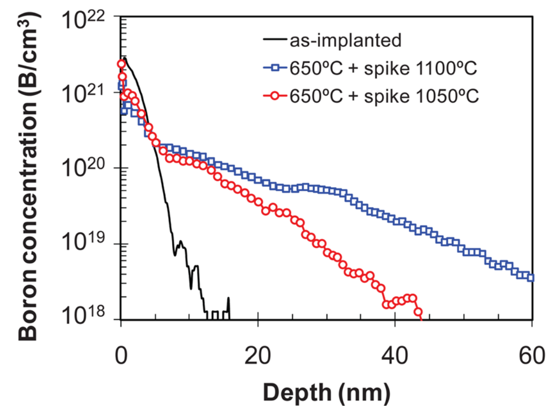

FIG. 4. (Color online) Simulated depth profiles for crystalline Si samples implanted with 500 eV B ions to a dose of 1×10^{15} B/cm^2 and subsequently annealed at 650 °C for 10 s (pre-stabilization annealing step) and then spike annealed at 1050 °C and 1100 °C using a 250 °C/s ramp-up rate. Simulations evidence the presence of a characteristic B concentration peak at a depth of ∼2 nm, in agreement to experiments [13], typically associated to the formation of BICs. As the thermal budget increases, the B concentration peak decreases and the tail region of the B profile broadens, similarly to experimental SIMS profiles [13].

Author complimentary copy. Redistribution subject to AIP license or copyright, see http://jap.aip.org/jap/copyright.jsp

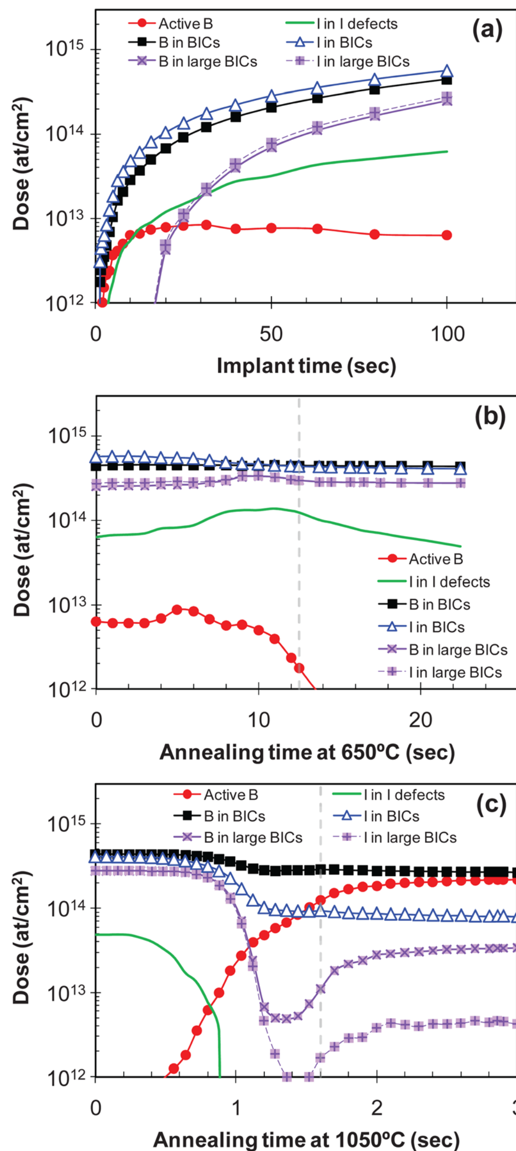

FIG. 5. (Color online) Simulated time evolution of the doses of electrically active B, Si Is stored in Si interstitial defects, B atoms and Is stored in BICs (both small and large BICs) and B atoms and Is stored in large BICs, as extracted from simulation of a crystalline Si sample implanted with 500 eV B ions to a dose of 1×10^{15} B/cm^2. This figure includes the evolution of doses during (a) the B implant at room temperature, (b) the pre-stabilization annealing step at 650 °C for 10 s using a 250 °C/s ramp-up rate, and (c) the second step spike annealing at 1050 °C using a 250 °C/s ramp-up rate. Dashed lines represent the end of the ramp up to the target temperatures.

During the B implant, a significant dose of B is already immobilized in BICs, as occurred in simulations performed by using previous models for BICs.[5] It can be observed that the Si interstitial dose trapped in BICs is higher than the B dose retained in BICs. This indicates that BICs with a high Si interstitial content have been formed. A fraction of the initial Si Is is also stored in Si self-interstitial defects (small and medium Si interstitial clusters) during the implant, but this amount is significantly lower than the dose of Is in BICs due to the presence of a very high B concentration. This is consistent to experimental observations indicating that the formation of large {113} interstitial defects is inhibited in the presence of high B concentrations.[29] It can be also observed that large BICs are also formed during the B implant, in agreement to experimental observations which shows that large BICs form quickly.[13] The dose of Is trapped in large BICs is also higher than the dose of B atoms stored in BICs which evidence that the large BICs formed in this simulation are rich in Is (mainly B_nI_m with $m \geq n$, contained in the region LBHI in Fig. 1). No big changes are observed during the temperature ramp up (at 50 °C/s) and annealing at 650 °C (Fig. 5(b)). Some emission of Si Is from interstitial defects is observed which leads to a reverse annealing behavior that causes additional B deactivation by the growth of existing BICs. Moreover, a loss of Is stored in BICs occurs due to some emission of Is from BICs as well as the eventual interaction of BICs with vacancies. During the spike annealing at 1050 °C, Si interstitial defects quickly dissolve, even during the temperature ramp up (at 250 °C/s, up to 1.6 s). On the other hand, BICs tend to emit Is, as it can be observed in the rapid decrease of the Is trapped in BICs. Furthermore, BICs also start to emit B_i resulting in a decrease of the clustered B dose and the consequent increase of the substitutional (active) B dose. Simulations show that the initial decrease in the interstitial clustered dose is faster than the decrease in the B clustered dose. According to our model, the faster decrease in the dose of Is trapped in BICs is due to a faster emission of Is from small BICs than B_i, resulting in small BICs with fewer Is than B atoms. However, in the case of large BICs the decrease in the dose of Is trapped in BICs practically follows the decrease of B atoms stored in BICs. This is due to the relatively quick emission of B_i from these large BICs of the region LBHI that, as discussed in Sec. II A, easily return to small BIC configurations even at relatively low temperatures. Once the density of large BICs significantly decreases, B activation is mainly controlled by the dissolution of small BICs. The dissolution pathway for small BICs follows the reverse reactions in the low Si interstitial content pathway as occurred in previous models.[5] As a result of high temperature spike anneals a significant dose of B atoms activate through the dissolution of small BICs, leading to the experimentally observed decrease in the B peak concentration.

Simulations are able to capture main phenomena extracted from experiments reported in the literature by Cristiano *et al.*[13] In fact, WBDF images reported by these authors evidenced the formation of many observable BICs (that contain both B and Is) after the first annealing step at low temperature. In addition, although the characteristic immobile peak associated to BICs were still detected by SIMS after high temperature spike anneals (since an immobile characteristic B peak was still observed), these BICs were no observed by WBDF imaging, indicating that their size probably decreased below the detection limit. Note that, at least in our simulations, some large BICs are still present after high temperature spike annealing (mainly large configurations within the region LBLI) but the density of these large BICs is very small and it could be practically negligible to be seen in experiments.

III. BICs KINETICS IN PREAMOPHIZED SILICON: EXPERIMENTAL DATA AND MODELING

Although the formation of BICs with sizes larger than generally assumed has been observed under different

Author complimentary copy. Redistribution subject to AIP license or copyright, see http://jap.aip.org/jap/copyright.jsp

experimental conditions (detected by electron microscopy techniques), to our knowledge all of them considered crystalline Si samples. The use of preamorphized Si samples is increasingly more demanded for the fabrication of ultrashallow and extremely highly doped junctions. Therefore, a possible identification and understanding of experimental conditions in which very stable large BICs could form in preamorphized Si becomes crucial from a technological point of view. This could establish experimental conditions that should be avoided in order to prevent the formation of large and very stable configurations that could be very difficult to dissolve even at very high temperature anneals.

The implant energies and fluences typically used in preamorphizing implants for the fabrication of ultra-shallow junctions are such as the EOR defects region beyond the amorphous/crystalline interface is very close to the B profile.[7,8] The realization of subsequent anneals after recrystallization leads to B deactivation and diffusion.[5,7,8] However, experiments and simulations do not evidence any significant formation of observable large BICs under these experimental conditions. Experiments included in Sec. III A evidence that the evolution of small BICs in preamorphized Si toward very stable large BICs is possible under conditions where the EOR defect region is placed so far from the B profile that the flux of Si Is toward the B profile is very low. The results of the experiments will be interpreted in terms of BIC formation in amorphous Si and transition to the crystalline phase (Sec. III B) and subsequent evolution as usual in crystalline Si (Sec. III C), with further details on the evidenced deleterious effect of BICs on the hole mobility.

A. Experimental

Experiments were performed on n-type, Si Czochralski (100) wafers (resistivity 1.5–4 Ω cm). A pre-amorphization implant (PAI) was performed at liquid nitrogen (LN_2) temperature with 500 keV, 5×10^{15} Si^-/cm^2 plus 40 keV, 1×10^{15} Si^-/cm^2 ion beams, obtaining an amorphous layer extending from the surface down to ~ 950 nm (experimentally observed by TEM analysis). B implants at 12 keV, 3×10^{15} B/cm^2 (labeled as sample LB) or 26 keV, 2×10^{16} B/cm^2 (labeled as sample HB) were performed resulting in B profiles with maximum peak concentrations of 5×10^{20} B/cm^3 at the depth of $\sim$60 nm (estimated by SRIM[30]) for LB samples or 2×10^{21} B/cm^3 at the depth of $\sim$120 nm[30] for HB samples. Implanted B profiles and p-n junctions were entirely contained within 250 nm from the surface. Then, rapid thermal anneals (RTA) at 700 °C were performed under N_2 flux to induce fully recrystallization of the preamorphized layers. To investigate the evolution of the active B dose and BICs during post-regrowth anneals as a function of time after SPER, we annealed the samples at 850 °C or 1000 °C for times ranging from 1 to 10 000 s. Sheet resistance (R_S) was measured by four-point probe technique whereas Hall effect was used to determine the Hall active dose (N_H) and the Hall mobility (μ_H). These measurements were affected by an error of about 5%. The active B dose (N_a) and the carrier mobility (μ_p) were computed as follows: $N_a = N_H \times r_H$ and $\mu_p = \mu_H / r_H$, where r_H is the Hall scattering factor (0.75 for Si[20]). A 200 kV JEOL JEM 2010 F energy filtered transmission electron microscopy (EFTEM) equipped with a Gatan Image Filter was used to observe the thermal evolution of defects present in the sample and their chemical composition. This system consists of a conventional TEM coupled with an electron energy loss spectrometer.

B. Physical modeling

Prior to the analysis of experimental and simulation data we should make some considerations about modeling. The kinetics of the nucleation of BICs in amorphous Si is generally not modeled in detail. In turn, it is usually assumed as the initial conditions after SPER that BICs appear above 2×10^{20} B/cm^3 as evidenced from experimental data.[7,8] Obviously, the evolution of B activation and BICs during anneals after recrystallization is strongly dependent on the particular BIC configurations considered as starting conditions. Previous simulation work concluded that initial BICs after recrystallization should not contain a high amount of Is.[5,31] Otherwise, B deactivation and subsequent reactivation that takes place during subsequent anneals after SPER will occur faster than experimentally observed and, as a result, excessive broadening of B profiles would be also obtained. Moreover, simulations previously reported in the literature, in which B profiles with concentrations up to 5×10^{20} B/cm^3 were considered,[31] suggested that B_2, B_3, and B_3I clusters could be the most predominant configurations resulting after recrystallization. On the other hand, theoretical calculations reported by Mattoni and Colombo have characterized the formation kinetics of some BICs during recrystallization and found that BIC configurations with different sizes could appear during the evolution of recrystallized B-doped Si. In particular, these authors found that B_2I, B_3I, and B_4I_2 configurations could play the major role in recrystallized B-doped layers.[18] Thus, a possible scenario for BICs after recrystallization could be based on the formation in amorphous Si of diverse BIC configurations that are transferred to crystalline Si in the most stable configurations compatible with the energetics included in Fig. 1. Moreover, it is feasible that starting conditions for BICs after recrystallization could depend on B concentration. In fact, if we assumed a randomized B atoms distribution, the probability of two, three, or four B atoms being placed at a second neighbor distance in the Si lattice depends on B concentration. In addition, B diffusivity in amorphous Si was shown to be several orders of magnitude larger than in crystalline Si.[32]

In order to test this possibility, we considered theoretical 30 nm wide box-shaped and initially fully active B profiles with different B concentrations (higher than typical upper limit to active B concentration, 2×10^{20} B/cm^3, reported for low-temperature SPER[7,8]). Based on a random B distribution, the amount of BICs obtained when two or more B atoms are closer than second neighbor distance is significantly smaller than experimentally observed. However, some diffusion of B atoms in amorphous Si during recrystallization could favor the formation of higher concentrations of BICs. Then, for these theoretical B distribution simulations we assigned to B atoms a diffusivity according to the

Author complimentary copy. Redistribution subject to AIP license or copyright, see http://jap.aip.org/jap/copyright.jsp

experimental value recently reported in the literature for the migration energy of B in amorphous Si (3.0 eV).[32] A typical low-temperature SPER annealing at 650 °C for 5 s was subsequently applied in all cases which would be enough to fully regrow a 30 nm wide theoretical amorphous layer. These theoretical simulations are a rough simplification of the actual situation since it is considered that all B atoms could diffuse during the whole recrystallization process with the assigned diffusivity. Thus, it does not account for the transition from amorphous to crystal for B atoms during the regrowth. However, this simplification could provide us a rough estimation of the size distribution of BICs in terms of number of B atoms per BIC (according to the distribution of B atoms) after recrystallization. Figure 6 includes the simulated electrically active B concentration and the ratio of "groups" with two, three, or four B atoms as a function of B concentration obtained under these theoretical conditions. The probability of having larger groups is practically negligible and for this reason groups with more than four B atoms are not considered in our analysis. Simulations lead to an electrically active B concentration around 2×10^{20} B/cm^3, in very good agreement with the experimental reported value for low-temperature SPER.[7,8] Regarding the ratio of the different "groups" of B atoms, simulations show that the group of two B atoms has the highest probability at the lower B concentration. As B concentration increases "groups" containing three or four B atoms become more likely. Obviously, as mentioned before, once these "groups" are transferred to crystalline Si BICs resulting after SPER should be compatible with energies included in Fig. 1. According to our B clustering model, B_2, B_3I, B_4I, and B_4I_2 are the configurations with lower energy and thus, they are the most energetically favored configurations.

Based on these features, we considered that for LB samples, in which B peak concentration is around 5×10^{20} B/cm^3, BICs after SPER are mainly in the form of B_2 (∼78%), B_3I(∼17%) and B_4I and B_4I_2 (∼5%), whereas for HB samples, with B peak concentration around 2×10^{21} B/cm^3, we considered B_2 (∼49%), B_3I(∼27%) and B_4I and B_4I_2 (∼24%). In fact, these conditions lead to the best fitting between simulations and experimental data. Note that once these BICs are transferred into crystalline Si after recrystallization their subsequent evolution takes place in crystalline Si, and thus, it is modeled according to energetics included in Fig. 1.

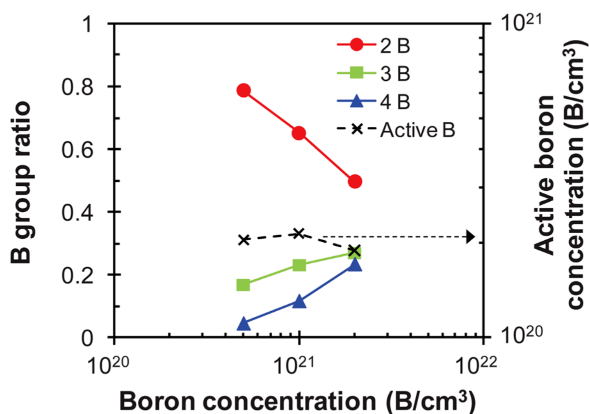

FIG. 6. (Color online) Electrically active B concentration and the ratio of groups with two, three, or four B atoms resulting after low-temperature SPER theoretical simulations as a function of B concentration. Simulations lead to an electrically active B concentration around 2×10^{20} B/cm^3, in very good agreement with the experimental reported value for low-temperature SPER [7, 8]. Group of two B atoms has the highest probability at the lower B concentration whereas groups containing three or four B atoms become more likely as B concentration increases.

C. Results and discussion

In order to investigate the evolution of the electrically active B dose during anneals after SPER, we have compared experimental data with our simulations. Figure 7 shows the time evolution of experimental N_a (symbols) for LB (Figs. 7(a) and 7(c)) and HB (Figs. 7(b) and 7(d)) samples during anneals at 850 °C (Figs. 7(a) and 7(b)) and 1000 °C (Figs. 7(c) and 7(d)) after SPER, as extracted from Hall measurements. These figures also include results for N_a extracted from two different types of simulation: one of them considered our previous model for BICs that only included small BICs (dashed lines) and other set of simulations were done by using the full extended model for BICs presented in this article (solid lines). Experiments indicate that a small fraction of the initially active B atoms slightly deactivates during anneals at 850 °C for both LB and HB samples (Figs. 7(a) and 7(b)). At 1000 °C, a fraction of the initially inactive (clustered) B atoms activates for both LB and HB samples (Figs. 7(c) and 7(d)). At this high temperature, in the case of LB sample the rate of B reactivation decreases as the annealing time increases, whereas for HB sample B initially slightly activates, but later on the annealing B deactivates. A comparison between experiments and simulations reveals that a more accurate agreement is obtained when the full extended model is considered. Moreover, larger discrepancy between simulations with previous and extended model is observed at high temperature anneals, being the difference more significant for the HB sample. This indicates that a significant effect of large BICs only occurs after intense thermal budgets under these experimental conditions.

The analysis of simulations show that during anneals at 850 °C B deactivation is mainly controlled by thermally generated Si Is for both LB and HB samples, since EOR defects are far enough (at ∼950 nm) to avoid their interaction with the B profile (projected range at ∼120 nm).[33] Simulations also show that the main mechanism for B deactivation is the interaction of Si Is (which are predominantly equilibrium Si Is under these conditions) with electrically active B atoms to form mobile B_i pairs that at the same time are able to interact with preexisting BICs by forward reactions given by Eq. (2). Since the transport capability of equilibrium Si Is has a high activation energy (formation energy + migration energy),[25] only a small fraction of B atoms deactivates and it occurs at a slow rate. During anneals at 1000 °C simulations indicate that B slightly reactivates at the beginning of the annealing for LB and HB samples, due to the faster dissolution rate of small BICs compared to their formation rate at high temperatures.[34] However, for long time anneals some B deactivation is again observed for HB sample. Note that for LB sample

Author complimentary copy. Redistribution subject to AIP license or copyright, see http://jap.aip.org/jap/copyright.jsp

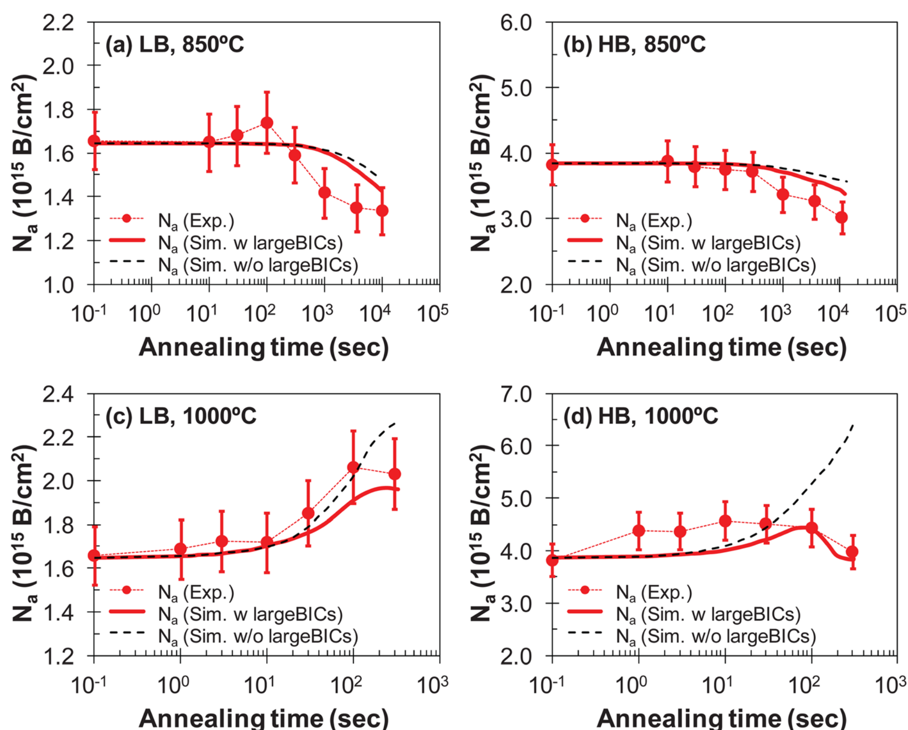

FIG. 7. (Color online) Evolution of the experimental (symbols) and simulated (lines) electrically active B dose as a function of annealing time for (a and c) LB (12 keV, 3×10^{15} B/cm^2) and (b and d) HB (26 keV, 2×10^{16} B/cm^2) samples during anneals at (a–b) 850 °C and (c–d) 1000 °C performed after SPER. Two different types of simulation are considered: dashed lines represent simulations performed by using our previous model for BICs (which only included small BICs) whereas solid lines correspond to simulations performed by using our full extended model for BICs (which shows a better agreement with experimental data).

no significant B deactivation is observed for long annealing time at 1000 °C although some deceleration in B reactivation seems to occur. Simulations indicate that the observed B deactivation or the decrease in the B activation rate observed at long time anneals for HB and LB samples, respectively, is due to the evolution of a fraction of small BICs (such us B_4) toward larger and more stable configurations (such as B_6I, B_7I, etc.) that are able to form in the presence of such a high B concentration after intense thermal budgets.

Note that the differences observed in Fig. 7 between the simulated active B doses with and without considering the extended model for BICs approximately correspond to the dose of B atoms stored in large BICs obtained by simulations. Thus, simulations indicate that the evolution from small BICs toward large configurations becomes significant at very high B concentrations such as those present in HB sample. This fact has been also experimentally confirmed by EFTEM analyses. Figure 8 includes cross section view EFTEM images obtained from the HB sample annealed at (Fig. 8(a)) 850 °C, 10 000 s and (Fig. 8(b)) 1100 °C, 30 s. These images were obtained by using a 4-eV-wide energy window for the plasmon loss peak centered at 22 eV, in order to maximize the cluster contrast with respect to the surrounding matrix. Such energy can be related to the plasmonic loss into these clusters. EFTEM demonstrates the absence of any relevant BIC (with size less than 1–2 nm) just after the SPER anneals at 700 °C for both LB and HB samples (not shown in the figure). However, the formation of large clusters in correspondence of the B peak depth is evident for HB samples annealed at 850 °C and 1100 °C (Figs. 8(a) and 8(b), respectively). In contrast, for LB samples EFTEM do not reveals in any case appreciable clustering. A B chemical map obtained by selecting the Boron K edge centered at 180 eV for the HB sample annealed at 1100 °C for 30 s is also included in Fig. 8(c). This analysis definitely proves that clusters are rich in B atoms. These analyses also indicate that these large BICs are very stable since they survive after very intense anneals as it is shown in Fig. 8(b) and 8(c).

A quantitative analysis of the EFTEM data allowed a determination of the size of the observed BICs in HB

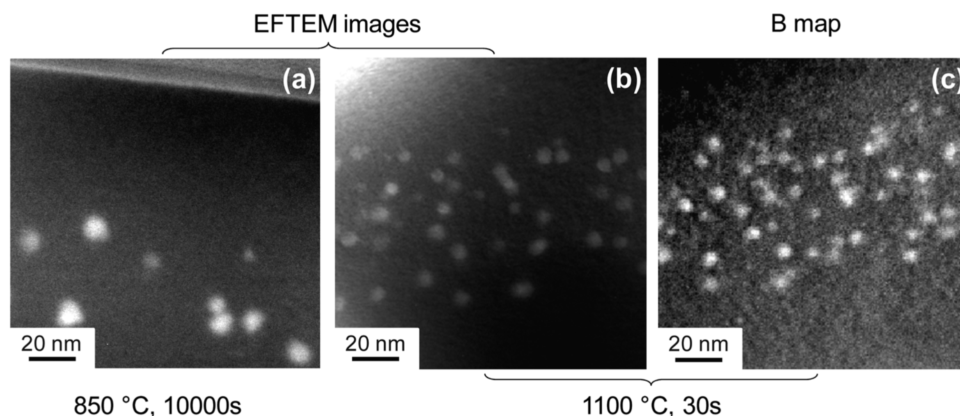

FIG. 8. EFTEM images of the HB sample annealed at (a) 850 °C, 10 000 s and (b) 1100 °C, 30 s obtained by selecting the plasmon loss peak centered at 22 eV and by a 4-eV-wide energy slit. (c) B chemical map obtained by selecting the Boron K edge centered at 180 eV for the sample annealed at 1100 °C for 30 s. EFTEM images evidences (a) the formation of large BIC configurations after annealing at 850 °C for 10 000 s, which are very stable since (b) they survive after very intense annealing at 1100 °C, 30 s. The comparison between images (b) and (c) indicates that the observed defects are rich in B atoms.

Author complimentary copy. Redistribution subject to AIP license or copyright, see http://jap.aip.org/jap/copyright.jsp

samples. Thus, for the sample annealed at 850 °C for 10 000 s a mean diameter of (8 ± 1) nm was obtained whereas for sample annealed at 1100 °C for 30 s the mean diameter decreases down to (5 ± 1) nm. In addition, it has been possible to calculate concentrations of BICs per unit volume for both samples. Indeed, the electron energy loss technique (EELS), used to collect an energy loss spectrum in the obtaining of EFTEM images, provides a convenient way to estimate the local thickness of the analyzed sample by a straightforward integration of the EELS signal[35] and the knowledge of the electron mean free path for inelastic scattering in the TEM sample.[36] Thus, for the HB sample annealed at 850 °C for 10 000 s the density of the observed BICs was about $(2.1 \pm 0.3) \times 10^{16}$ BICs/cm^3 whereas the density increases up to $(1.2 \pm 0.3) \times 10^{17}$ BICs/cm^3 after 1100°C for 30 s.

Assuming that large BICs are approximately spherical while atoms are disposed as in the Si lattice, and considering the mean volume of observable BICs, we may estimate the mean number of atoms contained in these BICs. This rough calculation estimates that these BICs could contain thousands or even tens of thousands of atoms. However, in our simulations we consider configurations for large BICs only up to 8 B atoms and some Is, thus containing a significantly lower number of atoms than the estimated mean number of atoms. In fact, these large BICs contain a number of atoms prohibitive for our atomistic simulations. Thus, our extended model for BICs represents a simplified model which is able to capture the main behavior of large BICs avoiding the need of including such large BICs as those experimentally observed.

Finally, another interesting feature revealed by the analysis of experimental data at high B concentrations is an apparent "anomalous" behavior of R_S and N_a at long time anneals. This anomalous behavior is shown in Fig. 9(a) (marked with ovals) which plots the evolution of R_S and N_a extracted from Hall measurements from HB samples at different instants during anneals at 850 °C and 1000 °C. Experimental data indicate that R_S and N_a initially evolve with opposite trends, as it is expected assuming that μ_p is almost constant during N_a evolution if high electrically active B concentrations are present.[19] However, at long time anneals at 850 °C both R_S and N_a decrease whereas at long time anneals at 1000 °C R_S remains approximately constant at the same time that N_a decreases, thus both situations suggest that μ_p is not constant during anneals (according to Eq. (1)).

We have investigated the evolution of μ_p extracted from Hall measurements during annealing, since it also affects the evolution of R_S. Generally, by considering Coulomb scattering it is assumed that μ_p is mostly dependent on the electrically active (ionized) dopant concentration.[19] Thus, from the analysis of the evolution of the concentration of electrically active B it is possible to infer the evolution of μ_p by using the analytical expression reported by Masetti *et al.*[19] In order to analyze the evolution of active B concentration during anneals at 850 and 1000 °C, we could estimate the maximum active B concentration level ($[\mathrm{B_{act}}]^{max}$) that corresponds to each measured N_a value during annealing. Since the B implant conditions used here result in quite spread B profiles, we could assume that B diffusion during annealing is negligible (B diffusion length is in the order of 10-15 nm after 850°C 10 000s annealing and it is approximately 20–25 nm after 1000 °C, 300s annealing[37]) compared to the junction depth (∼200 nm) which hardly modifies the B peak concentration. Based on this assumption, we could obtain N_a by integrating the as-implanted B profile below a certain $[\mathrm{B_{act}}]^{max}$ value. Even if some B diffusion had occurred, the B profile would become broader and with lower $[\mathrm{B_{act}}]^{max}$. This potentially overestimates the $[\mathrm{B_{act}}]^{max}$at longer annealing times. Finally, from the estimated values for $[\mathrm{B_{act}}]^{max}$, μ_p values could be estimated by using the expression reported by Masetti *et al*. (values estimated by this method are denoted as

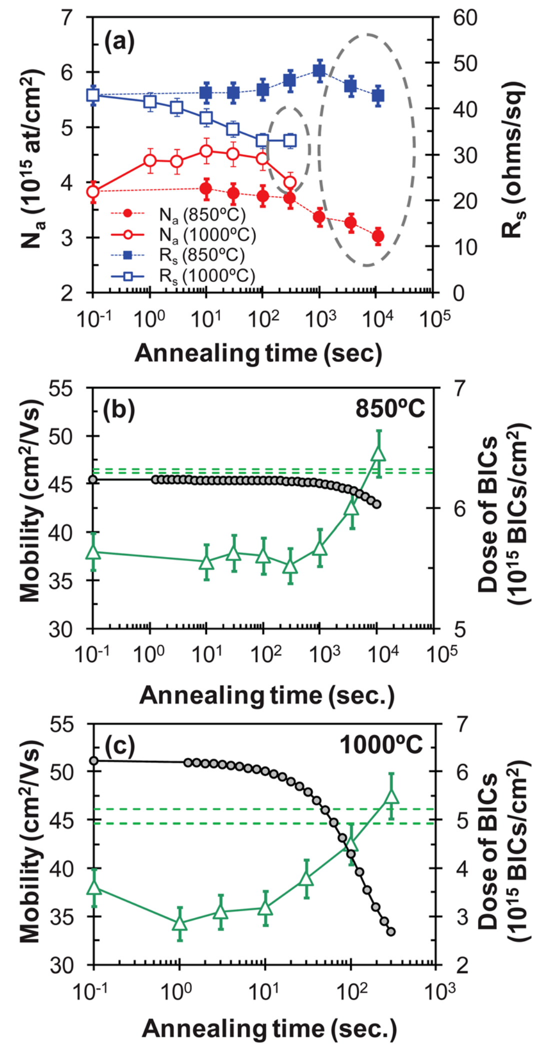

FIG. 9. (Color online) Time evolution of experimental (a) sheet resistance and active B dose and (b and c) hole mobility as extracted from Hall measurements for HB sample during anneals at 850 °C and 1000 °C performed after SPER. The simulated time evolution of the dose of BICs during anneals is also included. Experiments indicate that sheet resistance and active B dose initially evolve with opposite trends, as it has been generally assumed. However, at long time anneals an "anomalous" behavior (marked with ovals) is observed, since the active B dose decreases at the same time that sheet resistance also decreases (large oval, 850 °C) or remains approximately constant (small oval, 1000 °C), contrary to expected. This apparently "anomalous" behavior is due to the high increase in mobility observed at long time anneals, contrary to the expected small range of variation of mobility (marked with dashed lines and estimated through Masetti's expression [19]). A correlation between the high increase in mobility and the high decrease in the simulated density of BICs is observed. This suggests that mobility could be degraded by the presence of large densities of BICs.

Author complimentary copy. Redistribution subject to AIP license or copyright, see http://jap.aip.org/jap/copyright.jsp

μ_p^{Masetti}) which assumes that hole mobility only depends on electrically active B concentration.[19] Figures 9(b) and 9(c) include the time evolution of experimental μ_p (extracted from Hall measurements) during anneals at 850 °C (Fig. 9(b)) and 1000 °C (Fig. 9(c)) SPER for HB sample. For comparison, the expected estimated range of variation of μ_p^{Masetti} is also marked schematically in the figure. At both annealing temperatures the predictions for μ_p indicate that it should experience very small variations during annealing, according to the behavior generally assumed.[38] Nevertheless, in spite of the fact that the estimated values predict changes in μ_p^{Masetti} lower than 5% during both anneals experiments show a significant μ_p increase (~30%) at long time anneals for both annealing temperatures. This unexpected high increase in μ_p observed at long time anneals is responsible of the "anomalous" behavior observed in Fig. 9(a). Moreover, at short annealing times, the μ_p measured is significantly lower than expected from Masetti *et al.* whereas at long time anneals better agreement between experimental and expected μ_p is observed. These results suggest that some relevant difference may exist between short and long time annealed samples which should be responsible for μ_p degradation at short annealing times. In order to find a possible source for the observed μ_p degradation we have also included in Figs. 9(b) and 9(c) the time evolution of the simulated density of BICs obtained during anneals at 850 °C (Fig. 9(b)) and 1000 °C (Fig. 9(c)). Simulations show that the density of BICs is almost constant at the initial stages of the annealing, and it rapidly decreases at long time anneals. These results suggest that initially the large density of BICs may degrade μ_p at levels even smaller than the values predicted by Masetti *et al.* During annealing the total density of BICs decreases (through evolution to larger sizes or through dissolution of small BICs), and μ_p is significantly modified in such a way that variations in μ_p largely affect the R_S value.

Recently, Severac *et al.* have suggested that BICs could act as additional scattering centers with respect to ionized dopants and phonons, which should be added to Matthiessen's rule as an additional scattering mechanism.[39] In a similar sense, Clarysse *et al.* reported some deviations between experimental and theoretical values for μ_p in samples containing BICs, and they attributed this deviation to the presence of electrically inactive B atoms.[40] Our simulations evidenced a clear correlation between the evolutions of the density of BICs and μ_p. Thus, the large density of BICs obtained in simulations at short annealing times may act as additional scattering centers, lowering μ_p at levels even smaller than the values predicted by Masetti *et al.*, whereas the decrease in the density of BICs obtained at long time anneals could make their effect in μ_p practically negligible. Note that the decrease in the density of BICs could be underestimated in our simulations, since for simplicity we considered in our model large BICs significantly smaller than those observed experimentally. Moreover, it is worthy to note that Severac *et al.* have also found that the presence of high concentrations of BICs could affect not only μ_p but also the Hall scattering factor r_H that should be used in Hall measurements data extraction,which again affects the μ_p value.[41] In particular these authors found that the generally assumed value for r_H in Si ($r_H = 0.75$) should be increased up to values around 0.95 under particular experimental conditions in which very high concentrations of BICs are present. The authors again attributed this increase in r_H to the possible presence of additional scattering centers that can suppose the existence of very large concentrations of BICs. Nevertheless, the experimental data extracted by Hall measurements included in this article considered the generally assumed value for r_H in Si ($r_H = 0.75$). Note that if a higher value for r_H were considered in our experimental data for annealing times at which the density of BICs is very high (i.e., data at short time annealed samples), μ_p values at these instants would be even more degraded. This would make the variations in mobility during annealing even more significant, thus making the general assumption of small variations in μ_p during N_a and R_S evolution even more erroneous.

Another possible effect on μ_p could due to strained Si considerations. Romano *et al.* have investigated the origin of the experimentally observed dependence of μ_p on the dopant species in heavily B-doped Si.[42] These authors suggested that the relatively high μ_p values experimentally observed in highly B-doped Si (at concentration higher than 10^{19} B/cm^3), which has been analytically expressed by Masetti *et al.*, is due to the tensile strain induced by substitutional B which increases μ_p. On the other hand, Bisognin *et al.* have evidenced that BICs could induce compressive strain which is found to be proportional to the clustered B amount.[43] Therefore, the compressive strain induced by the large density of BICs obtained in simulations at short annealing times could partially compensate the tensile strain of substitutional B, thus degrading μ_p toward unstrained Si mobility values.

IV. CONCLUSIONS

An extended model for B clustering in Si have been developed, which accounts for the eventual enhanced stability of BICs for high B concentrations while still maintaining the validity of previous models for low and medium B concentrations. In order to account for different evolutions of BICs observed under diverse experimental conditions, four main regions or type of B_nI_m configurations have been defined in the model: a region that includes small BICs ($n \leq 4$) that reproduce experimental data at low and medium B concentration; a region that considers very stable large BICs ($n > 4$, $m \ll n$) that form only in the presence of high B concentration and low flux of Si Is; a region that includes less stable large BICs ($n > 4$ and large amount of Is) that can form in the presence of high B concentration and high flux of Si Is; and finally, a region that considers quite unstable large BICs ($n > 4$ and intermediate amount of Is) that act as a barrier among less stable and very stable large BICs.

Experimental data complemented with an atomistic KMC simulation study on B activation in preamorphized Si in such a way that EOR defects are far from the B profile have been also presented. Simplified simulations that include the recently experimentally deduced value of B diffusivity in amorphous Si have allowed us to simulate the BIC formation in amorphous Si and estimate the BIC configurations that with more probability result after recrystallization of preamorphized

Author complimentary copy. Redistribution subject to AIP license or copyright, see http://jap.aip.org/jap/copyright.jsp

layers containing high concentration B profiles. Our simulations suggest B_2, B_3I, B_4I, and B_4I_2 small BIC configurations as the more probable and energetically favored BICs after recrystallization, with ratios that depend on B concentration. Under these conditions simulations show that B deactivation during anneals after SPER occurs through the interaction of thermally equilibrium Si Is with active B atoms, leading to the formation of B_i pairs that are able to interact with pre-existing small BICs. EFTEM images and simulations indicate that a significant fraction of the pre-existing BICs evolve into large and very stable BIC configurations if very high B concentrations are present. Moreover, Hall measurements combined with simulations indicate that the presence of large densities of BICs in highly B-doped samples implies a significant degradation of hole mobility. As a consequence, the value of the sheet resistance, and thus the device performance, is not only determined by the amount of electrically active B dose, but also by the electrically inactive BICs. This result is very relevant in the evaluation of sheet resistance and dopant activation, since the generally assumed opposite evolution of these magnitudes—by considering negligible changes in hole mobility—could lead to erroneous conclusions.

ACKNOWLEDGMENTS

This work was supported by the MICINN under Project TEC2008-06069, and by the Consejería de Educacion y Cultura de la JCYL under Project No. VA011A09. The authors wish to thank C. Percolla and S. Tatì (MATIS-IMM-CNR) for technical expert assistance.

[1]See International Technology Roadmap for Semiconductors, http://public.itrs.net (2010).
[2]A. Armigliato, D. Nobili, P. Ostoja, M. Servidori, and S. Solmi, in *Semiconductor Silicon 1977*, edited by H. Huff and E. Sirtl (The Electrochemical Society, Princeton, NJ, 1977), Vol. 77-2, pp. 638.
[3]S. C. Jain, W. Schoenmaker, R. Lindsay, P. A. Stolk, S. Decoutere, M. Willander, and H. E. Maes, J. Appl. Phys. **91**, 8919 (2002).
[4]L. Pelaz, G. H. Gilmer, H.-J. Gossmann, J. M. Poate, C. S. Rafferty, M. Jaraiz, and J. Barbolla, Appl. Phys. Lett. **74**, 3657 (1999).
[5]M. Aboy, L. Pelaz, L. A. Marques, P. Lopez, and J. Barbolla, J. Appl. Phys. **97**, 103520 (2005), and references therein.
[6]A. Mokhberi, P. B. Griffin, J. D. Plummer, E. Paton, S. McCoy, and K. Elliott, IEEE Trans. Electron Devices **49**, 1183 (2002).
[7]J.-Y. Jin, J. Liu, U. Jeong, S. Mehta, and K. Jones, J. Vac. Sci. Technol. B **20**, 422 (2002).
[8]F. Cristiano, N. Cherkashin, P. Calvo, Y. Lamrani, X. Hebrasa, A. Claverie, W. Lerch, and S. Paul, Mater. Sci. Eng. B **114-115**, 174 (2004).
[9]X.-Y. Liu, W. Windl, and M. P. Masquelier, Appl. Phys. Lett. **77**, 2018 (2000).
[10]T. J. Lenosky, B. Sadigh, S. K. Theiss, M. J. Caturla, and T. D. de la Rubia, Appl. Phys. Lett. **77**, 1834 (2000).
[11]W. Luo and P. Clancy, J. Appl. Phys. **89**, 1596 (2001).
[12]P. Alippi, P. Ruggerone, and L. Colombo, Phys. Rev. B **69**, 125205 (2004).
[13]F. Cristiano, X. Hebras, N. Cherkashin, A. Claverie, W. Lerch, and S. Paul, Appl. Phys. Lett. **83**, 5407 (2005).
[14]S. Boninelli. S. Mirabella, E. Bruno, F. Priolo, F. Cristiano, A. Claverie, D. De Salvador, G. Bisognin, and E. Napolitani, Appl. Phys. Lett. **91**, 031905 (2007).
[15]D. De Salvador, E. Napolitani, G. Bisognin, A. Carnera, E. Bruno, S. Mirabella, G. Impellizzeri, and F. Priolo, Mater. Sci. Eng. B **124-125**, 32 (2005).
[16]V. C. Venezia, R. Duffy, L. Pelaz, M. J. P. Hopstaken, G. C. J. Maas, T. Dao, Y. Tamminga, and P. Graat, Mater. Sci. Eng. B **124-125**, 245 (2005).
[17]D. DeSalvador, G. Bisognin, M. Di Marino, E. Napolitani, A. Carnera, H. Graoui, M. A. Foad, F. Boscherini, and S. Mirabella, Appl. Phys. Lett. **89**, 241901 (2006).
[18]A. Mattoni and L. Colombo, Phys. Rev. B **69**, 045204 (2004).
[19]G. Masetti, M. Severi, and S. Solmi, IEEE Trans. Electronic Devices **30**, 764 (1983).
[20]L. Romano, E. Napolitani, V. Privitera, S. Scalese, A. Terrasi, S. Mirabella, and M. G. Grimaldi, Mater. Sci. Eng. B **102**, 49 (2003).
[21]L. Pelaz, L. A. Marqués, M. Aboy, P. López, and J. Barbolla, Comp. Mater. Sci. **33**, 92 (2005).
[22]G. H. Gilmer, T. Diaz de la Rubia, D. M. Stock, and M. Jaraiz, Nucl. Instrum. Methods B **102**, 247 (1995).
[23]A. Bongiorno, L. Colombo, and T. Diaz de la Rubia, Europhys. Lett. **43**, 695 (1998).
[24]B. Sadigh, T. J. Lenosky, S. K. Theiss, M.-J. Caturla, T. Diaz de la Rubia, and M. A. Foad, Phys. Rev. Lett. **83**, 4341 (1999).
[25]H. Bracht, E. E. Haller, and R. Clark-Phelps, Phys. Rev. Lett. **81**, 393 (1998).
[26]N. E. B. Cowern, G. Mannino, P. A. Stolk, F. Roozeboom, H. G. A. Huizing, J. G. M. van Berkum, F. Cristiano, A. Claverie, and M. Jaraiz, Phys. Rev. Lett. **82**, 4460 (1999).
[27]More configurations with larger amount of B atoms and Si interstitial defects could be included in the model. In fact, experiments suggested that the observed large BICs could contain hundred of atoms. However, the inclusion of a large amount of stable BIC configurations in the model would complicate the parameter calibration enormously. Moreover, we have found that this simplification could be enough to describe the overall behavior evidenced by experimental data.
[28]S. Mirabella, E. Bruno, F. Priolo, D. De Salvador, E. Napolitani, A. V. Drigo, and A. Carnera, Appl. Phys. Lett. **83**, 680 (2003).
[29]T. E. Haynes, D. J. Eaglesham, P. A. Stolk, H.-J. Gossmann, D. C. Jacobson, and J. M. Poate, Appl. Phys. Lett. **69**, 1376 (1996).
[30]J. F. Ziegler, J. P. Biersack, and U. Littmark, *The Stopping and Range of Ions in Solids*, vol. 1 *Stopping and Ranges of Ions in Matter* (Pergamon, New York, 1984), See www.srim.org.
[31]M. Aboy, L. Pelaz, P. Lopez, E. Bruno, S. Mirabella and E. Napolitani, Mater. Sci. Eng. B **154-155**, 247 (2008).
[32]S. Mirabella, D. De Salvador, E. Bruno, E. Napolitani, E. F. Pecora, S. Boninelli and F. Priolo, Phys. Rev. Lett. **100**, 155901 (2008).
[33]In order to ensure that EOR defects are far enough and do not interact with B atoms, reference experiments (not shown in this article) were also performed on a 900 nm-wide, molecular beam epitaxy (MBE) grown, Si film containing a 50 nm-wide $Si_{1-y}C_y$ layer ($y = 0.3$ at.%) at a depth of 450 nm (which acts as a trap for Is). Experimental results with and without the $Si_{1-y}C_y$ were practically the same in all samples.
[34]M. Aboy, L. Pelaz, P. López, L. A. Marqués, R. Duffy, and V. C. Venezia, Appl. Phys. Lett. **88**, 191917 (2006).
[35]R. F. Egerton, *Electron Energy-Loss Spectroscopy in the Electron Microscope*, 2nd ed. (New York, Plenum, 1996).
[36]S. Boninelli, F. Iacona, Giorgia Franzò, C. Bongiorno, C. Spinella and F. Priolo, J. Phys.: Condens. Matter **19**, 225003 (2007).
[37]P. Pichler, in *Intrinsic Point Defects, Impurities, and Their Diffusion in Silicon*, edited by S. Selberherr (Springer, Wien, 2004).
[38]The systematically slight overestimation of $[B_{act}]^{max}$ at long annealing times (at which B diffusion is not negligible) leads us to slightly underestimated values for $\mu_p^{Masetti}$.
[39]F. Severac, F. Cristiano, E. Bedel-Pereira, P. F. Fazzini, J. Boucher, W. Lerch, and S. Hamm, J. Appl. Phys. **107**, 123711 (2010).
[40]T. Clarysse, J. Bogdanowicz, J. Goossens, A. Moussa, E. Rosseel, W. Vandervorst, D. H. Petersen, R. Lin, P. F. Nielsen, O. Hansen, G. Merklin, N. S. Bennett, and N. E. B. Cowern, Mater. Sci. Eng. B **154-155**, 24 (2008).
[41]F. Severac, F. Cristiano, E. Bedel-Pereira, P. F. Fazzini, W. Lerch, S. Paul, X. Hebras, and F. Giannazzo, J. Appl. Phys. **105**, 043711 (2009).
[42]L. Romano, A. M. Piro, M. G. Grimaldi, G. Bisognin, E. Napolitani, and D. De Salvador, Phys. Rev. Lett. **97**, 136605 (2006).
[43]G. Bisognin, D. De Salvador, E. Napolitani, A. Carnera, E. Bruno, S. Mirabella, F. Priolo, and A. Mattoni, Semicond. Sci. Techol. **21**, L41 (2006).

Author complimentary copy. Redistribution subject to AIP license or copyright, see http://jap.aip.org/jap/copyright.jsp